remote sensing

MDPI

Article

Operational Flood Mapping Using Multi-Temporal Sentinel-1 SAR Images: A Case Study from Bangladesh

Kabir Uddin [1,*], Mir A. Matin [1] and Franz J. Meyer [2]

[1] International Centre for Integrated Mountain Development, Kathmandu 44700, Nepal
[2] Geophysical Institute, University of Alaska Fairbanks, Fairbanks, AK 757500, USA
* Correspondence: Kabir.Uddin@icimod.org; Tel.: +977-1-527-5222

Received: 1 May 2019; Accepted: 23 June 2019; Published: 3 July 2019

Abstract: Bangladesh is one of the most flood-affected countries in the world. In the last few decades, flood frequency, intensity, duration, and devastation have increased in Bangladesh. Identifying flood-damaged areas is highly essential for an effective flood response. This study aimed at developing an operational methodology for rapid flood inundation and potential flood damaged area mapping to support a quick and effective event response. Sentinel-1 images from March, April, June, and August 2017 were used to generate inundation extents of the corresponding months. The 2017 pre-flood land cover maps were prepared using Landsat-8 images to identify major land cover on the ground before flooding. The overall accuracy of flood inundation mapping was 96.44% and the accuracy of the land cover map was 87.51%. The total flood inundated area corresponded to 2.01%, 4.53%, and 7.01% for the months April, June, and August 2017, respectively. Based on the Landsat-8 derived land cover information, the study determined that cropland damaged by floods was 1.51% in April, 3.46% in June, 5.30% in August, located mostly in the Sylhet and Rangpur divisions. Finally, flood inundation maps were distributed to the broader user community to aid in hazard response. The data and methodology of the study can be replicated for every year to map flooding in Bangladesh.

Keywords: flood mapping; damage assessment; SAR image; Sentinel-1; Landsat-8; Google Earth Engine; GEE; Bangladesh

1. Introduction

The Ganges, Brahmaputra, Meghna (GBM) basins are one of the most flood-prone basins in the world. Due to being part of such big basins and most of the area being less than 7 m above mean sea level, Bangladesh faces the cumulative effects of floods due to water flashing from nearby hills, the accumulation of the inflow of water from upstream catchments, and locally heavy rainfall enhanced by drainage congestion [1–4]. The country has a long history of destructive flooding that has had very adverse impacts on lives and property [5–7]. Approximately 20,000 deaths have been reported due to flooding from 1954–2007 [8]. An analysis by the Bangladesh Bureau of Statistics showed that from 2009–2014, 56.62% of households have been affected by disasters at least once [9]. Among them, 24.44% were affected by flood events. More than 80% of the country is flood prone [10]. In an average year, approximately 20–25% of the area of the country is inundated by floods, while in extreme years, the inundated area makes up more than 60% of the country [11]. During the 2017 flood, more than 30% of the country's areas were inundated, causing at least 134 deaths and affecting more than 5.7 million people [12]. Widespread frequent flooding is not only a profound problem for Bangladesh. Between 1995–2015, there was at least a $166 billion economic loss caused by different floods events around the world [13].

For effective response during flooding events, the rapid monitoring of flood situations, including mapping the extent of the inundation and damage, is highly critical [14,15]. Before any flood event, flood forecasting and simulation of the inundation extent is critical for risk mitigation [16]. At present, flood early warning and monitoring information is produced by the Flood Forecasting and Warning Centre (FFWC) as water levels change in major river systems in Bangladesh [5]. The extent of inundation is also mapped by comparing the water level with the national digital elevation model (DEM). Generating inundation maps from hydrological models requires an up-to-date and accurate DEM as well as computing infrastructure to model the effects of obstacles on the flow of flood water in the floodplains. Unfortunately, a sufficiently high accurate DEM and infrastructure data are often not available [17]. Flood management based on water level forecasting is not effective in providing a spatially distributed flood area for the timely monitoring of flood events [13,18]. Satellite-based monitoring of flood extent overcomes the limitations of the hydrological model-based approach [19]. Various attempts have been made in the past to map the flood extent in Bangladesh from satellite images [20]. Rasid and Pramanik [7] attempted comprehensive flood extent mapping of Bangladesh in 1980 using National Oceanographic Atmospheric Administrative's (NOAA) advanced very high resolution radiometer (AVHRR) data. Islam, et al. [21] used MODIS surface reflectance images for flood mapping for the years 2004 and 2007. Ahmed, et al. [22] used Landsat-8 and MODIS to determine the impact of a 2017 flash flooding event on rice production in the Haor area. MODIS images also have considerable potential for daily agriculture flood mapping of Bangladesh [23].

Although optical images have great potential for mapping during good weather conditions with image analysis capacity and accuracy [16,24–26], their use is limited to flood mapping in Bangladesh due to high (approximately 80%) cloud coverage during the monsoon and flood period. The average cloud coverage for Bangladesh was found to be 88.5% in June, 90.8% in July, 78.3% in August, 78.3% in September, and 17% in December (all at latitude: 24.921°N and longitude 91.869°E) [27]. In reality, the acquisition of cloud-free MODIS and Landsat optical images for flood mapping during flooding events is almost impossible. In April 2017, there were no cloud-free Landsat-8 images available for the study area for flood mapping. Similarly, during the period of 22 March–6 April 2017, MODIS images were not usable for mapping [22].

In Bangladesh, floods often occur when the sky is covered by clouds, thus making the utilisation of optical satellite images is infeasible in providing inundation mapping during the disaster. Therefore, spaceborne synthetic aperture radar (SAR) systems are the most preferred option for monitoring the flood condition. The introduction of SAR sensors has shown great potential for flood mapping due to their independence from solar illumination and very low dependency on atmospheric conditions [28]. Some studies have demonstrated that SAR images are useful for determining flood extent during a disaster [29–31]. An analysis of the benefits of using SAR images for flood mapping in Bangladesh was conducted using RADARSAT images from 1998–2004 and indicated strong applicability to flood response [32,33]. Using six scenes of RADARSAT images from 1988 (July–September) and available GIS database, Dewan, et al. [34] conducted a study on flood hazard mapping in Greater Dhaka. In support of ground data, Hoque, Nakayama, Matsuyama and Matsumoto [32] analyzed RADARSAT images to produce inundation maps from 2000–2004 and proposed unique flood hazard maps of the north-eastern region of Bangladesh. Using the same RADARSAT images of 1998 and 2004, another flood mapping study was conducted for the Kurigram district of Bangladesh [35]. Considering the published literature, none of the studies produced flood maps (2005 onward) with national coverage for damage assessment using Sentinel-1 and ALOS PALSAR images. However, the availability of free SAR data through the European Space Agency's (ESA) Sentinel-1 C-band SAR mission created a major opportunity for flood extent monitoring in developing countries such as Bangladesh.

For an estimation of flood damaged areas, pre-flood national level land cover is also essential. In the region, knowledge-based and object-based image analysis methods were used for the national land cover change assessment of Bangladesh [36], Bhutan [37], and Nepal [38,39]. These studies were mostly conducted at decadal intervals for addressing national environmental issues but are not

useful for analyzing flood damage assessment. Considering the amount of image downloading and processing required, the desktop based systems are not suitable for providing rapid processing services critical for a flood response. The cloud-based image processing platform from Google Earth Engine (GEE) is enabling the rapid processing of such big datasets covering a large area [40,41]. The GEE has publicly made available large amounts of remote sensing satellite data collection and provides image analysis functionality at large spatial scales [42].

In 2017, unpredicted early heavy rain caused flooding in several parts of Bangladesh and damaged pre-harvested crops in April [22]. The flood started in April and continued until the last week of August, causing substantial damage to housing, property, and infrastructure. As part of the rapid response, the disaster management agencies were in urgent need of information about the inundated areas to prioritize their relief and rescue activities [43,44]. This study aims to develop an operational methodology to support the response agencies by providing timely information on such inundated areas so as to prioritize emergency response activities. This study also aims to develop a methodology for potential damage assessment by analyzing pre-flood land cover maps automatically on the GEE platform. The inundation and flood damage data have been made publicly available for decision making processes related to flood management.

2. Materials and Methods

2.1. Study Area

Figure 1 shows the study area for rapid flood mapping and potential damage assessment in Bangladesh. Bangladesh encompasses the world's largest delta system located in the southern part of the foothills of the Himalayan mountain region and in the northern part of the Bay of Bengal, with a boundary between 20°N to 26°N and 88°N to 92°E with an area of 147,570 km^2 [45]. The southern part of the delta is occupied by the world's largest mangrove forest (the Sundarbans). The south-eastern part includes Bangladesh's main hilly region, while low hills characterize the north-east of Bangladesh and the remaining area is mainly plain land.

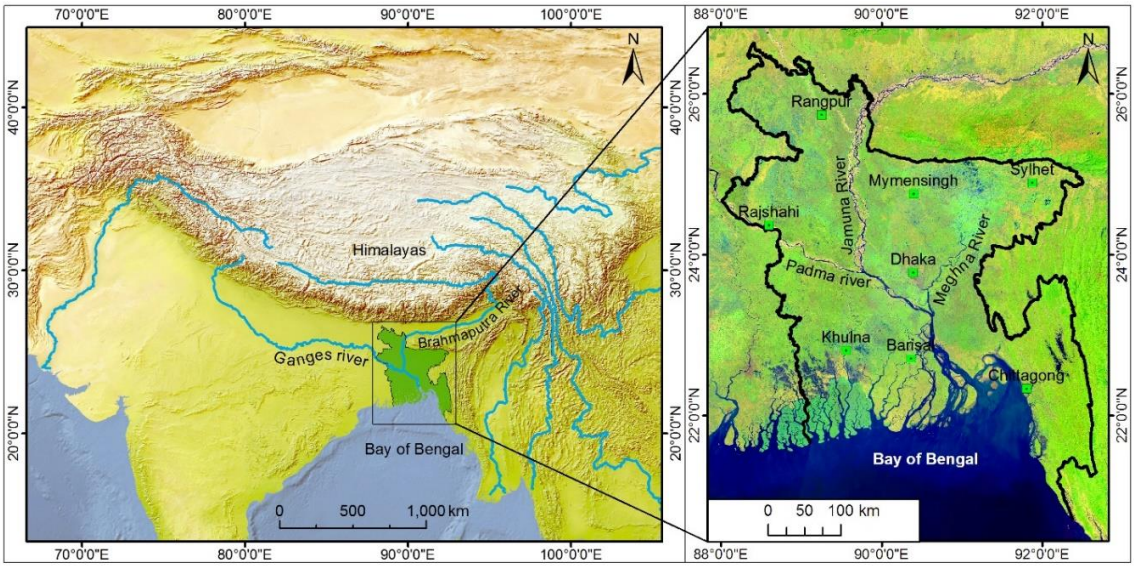

Figure 1. Study area of the entire country of Bangladesh showing three large river systems: The Ganges (Padma), Brahmaputra (Jamuna), and the Meghna forming the largest riverine delta in the world.

Approximately 50% of the country is within 7 m of mean sea level and most of the country is on a delta plain under the influence of the Padma, Jamuna, and Meghna rivers. Most of the plain lands is used for crop production and approximately 87% of rural households rely on agriculture for at least part of their income. Rice production in Bangladesh is a crucial part of the national economy. Recently,

Bangladesh has become one of the top 5 rice-producing countries in the world [46]. If no flood occurs in the coming year, Bangladesh will remain in the top 5 rice-producing countries. Although Bangladesh is a land of 6 seasons, the 3 most distinct seasons are the pre-monsoon hot season from March to May, the rainy monsoon season lasting from June through October, and a cool, dry winter season from November through February. The country has an average of 136 wet days per year, and approximately 80% of yearly rainfall occurs from June to September [47]. In a normal year, about one-third area of the country gets inundated by flood water [48]. The planet's highest rainfall occurs in Cherrapunji, which is located just a few kilometres away from the north-eastern border of Bangladesh. The high annual rainfall combined with the mountain terrain causes rivers from the north eastern border to flow with a very high current due to high gradient topography. When this water reaches Bangladesh territory, it spreads over a large area and regularly causes different levels of flood incidents in Bangladesh. Sometimes, locally concentrated prolonged heavy rainfall worsens the flood situations.

2.2. Materials

To enable comprehensive inundation mapping across Bangladesh, approximately 11 frames of Sentinel-1 C-band interferometric wide swath (IW) frames with a 250 km swath width were required (Figure 2).

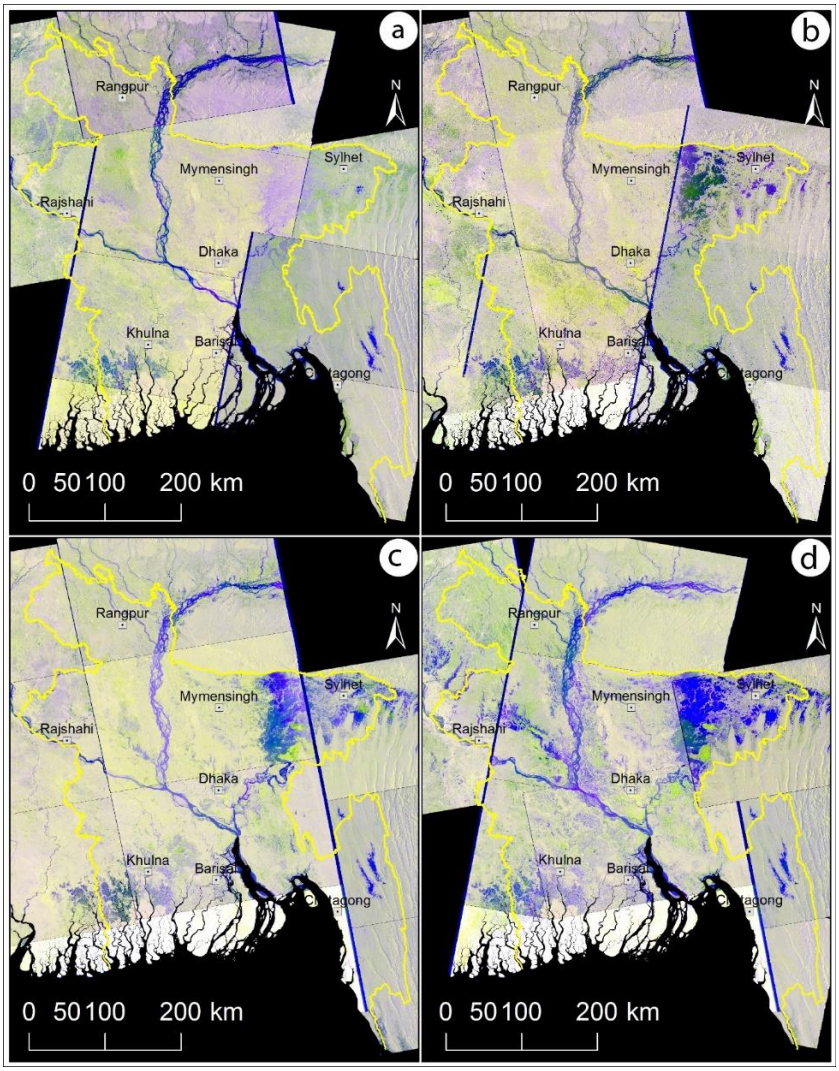

Figure 2. Sentinel-1 composites VH (red), VH (green), and VH/VV backscatter ratio (blue) images used for inundation mapping of (**a**) March, (**b**) April, (**c**) June, and (**d**) August 2017.

For the pre-flood (March) and post-flood (April, June, and August) inundation mapping, a total of 44 dual-polarization Sentinel-1 level-1 Ground Range Detected (GRD) products were used. The GRD products consist of focused SAR data that was detected, multi-looked, and projected to the ground range using the WGS-84 Earth ellipsoid model. The ellipsoid projection of the GRD products was corrected using the terrain height specified in the product's general annotation. Both the like-polarized (vertical transmit and vertical receive (VV)) and cross-polarized (vertical transmit and horizontal receive (VH)) channels were used in this study, and data were retrieved as Level-1 GRD products. Sentinel-1 SAR images were useful as the data were freely available within 3 h of acquisition for near real-time (NRT) emergency response and within 24 h for systematically archived data. Table S1 shows the Sentinel-1 images that were used in this study, which were freely downloaded from the Copernicus open access hub data portal of the European Space Agency (ESA).

In addition to SAR and as part of the flood damage assessment, pre-flood cloud-free Landsat-8 image collections between 1 January and 30 June 2017 were used for land use/land cover mapping in the Google Earth Engine. To support land cover classification, additional ancillary data used in this study included a 30-m resolution shuttle radar topography mission (SRTM) digital elevation models (DEM) [49], which were retrieved from the United States Geological Survey (USGS) archived data portal, as well as road network information from OpenStreetMap [50] and administrative boundary data from the database of Global Administrative Areas (GADM) [51].

2.3. Methods

The methods used for this study are presented in Figure 3. Specifically, Sentinel-1 image classification for flood mapping, with initial pre-processing carried out to mitigate the SAR-typical speckle noise signatures from the images. During the pre-processing step, we rectified the radiometric and geometric distortions due to the characteristics of the imaging system and imaging conditions and performed radiometric corrections to improve visualization and interpretation for flood mapping.

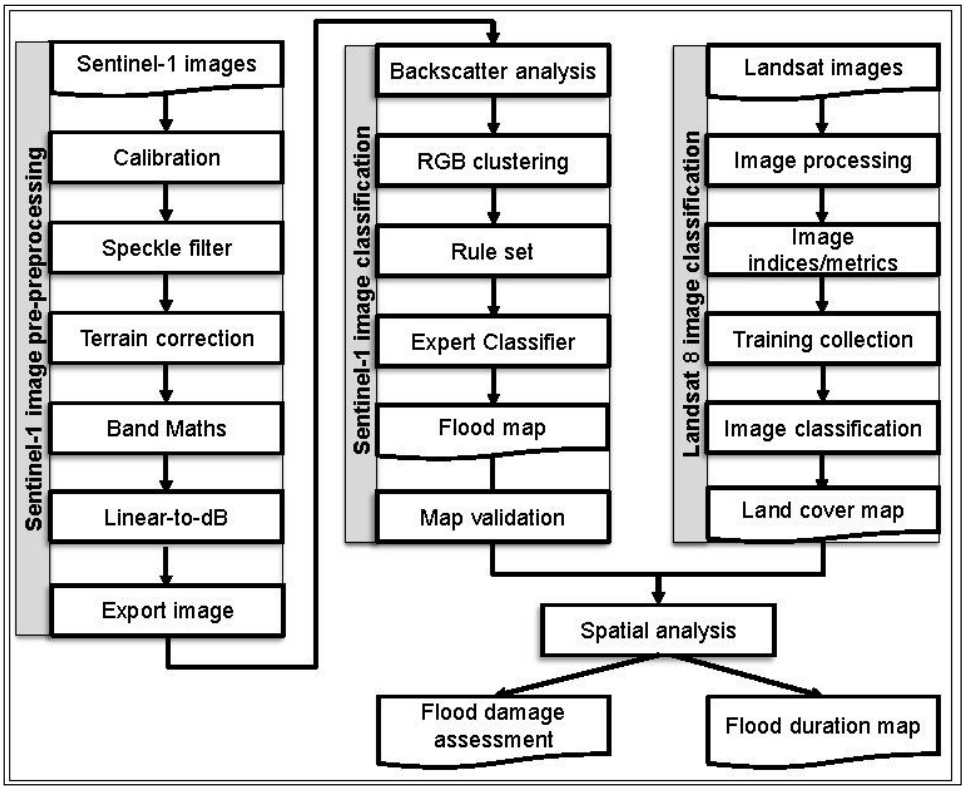

Figure 3. Overall methodological framework for the flood inundation mapping and damage assessment using multi-temporal Sentinel-1 and Landsat-8 satellite images.

The pre-processing steps, including data import, radiometric calibration, speckle filtering, radiometric terrain correction [52,53], linear-to-backscattering coefficient decibel scaling (dB) transformation, and data export, were implemented using ESA's Sentinel Application Platform (SNAP). The open-access SNAP toolbox is capable of reading, pre-processing, and visualizing Sentinel-1 SAR images.

During the Sentinel-1 pre-processing, Level-1 images were first imported into the SNAP Desktop tool. Secondly, Sentinel-1 images were radiometrically corrected by applying annotated image calibration constants to arrive at physically meaningful radar backscatter pixel values. Thirdly, speckle filters were applied to reduce the granular noise characteristic to SAR data. Fourthly, multi-look processing was carried out to reduce the speckle further and improve image interpretability. Fifthly, geometric distortions present in the SAR images were corrected by transforming the coordinates to a standard reference frame. The ratio band of VH/VV was generated dividing the VH by the VV band. Finally, a radiometric conversion from a linear scale to a dB scale was conducted using the following expressions:

$$\sigma^0_{dB} = 10 \cdot \log_{10} \sigma^0 \quad (1)$$

where, σ^0 (dB)—backscattering image in dB, σ^0—Sigma nought image.

The preprocessed images were exported for classification. For automation, all processing steps were assembled and connected through Graph Builder, which is available in SNAP and was run in batch processing mode. The pre-processed stack of Sentinel-1 SAR images was imported into ERDAS Imagine for knowledge-based image analysis. According to Janssen and Middelkoop [54], knowledge-based classifications contain the following 5 characteristics: Aim, ancillary data, domain knowledge, knowledge presentation, and inference. The knowledge engineer provides the interface for an expert with first-hand knowledge of the data to develop an algorithm into a hierarchical decision tree using logic or rules [55]. While performing expert classification, the Sentinel-1 images were clustered to create a thematic raster layer by RGB clustering functions in ERDAS Imagine. In geospatial applications, the unsupervised classification used to be known as the iso-clustering or migrating means technique that helps to group the same type of features into homogeneous and diverse features into heterogeneous clusters [56–58]. The RGB clustering is the most common technique for data compression and iso-clustering works better on an optimal number of classes usually unknown [59,60]. The RGB clustering functions are a simple classification algorithm that quickly compresses a three-band image into a single-band pseudo-colour image without necessarily classifying any particular features and without a signature file and decision rule. The RGB clustering provides greater control over the parameters used to partition the pixels into similar classes [61,62]. During Sentinel 1 image clustering, the VH band is designated as a red band, the VV band as a green band, and the VH/VV band as the blue band. Secondly, the RGB clustered image was processed to generate a clamped image for converting thematic class values into uniquely numbered "polygons", representing contiguous groups of the original class values. Thirdly, within the clamped image, mean radar backscatter (dB) values of the VH and VV bands were generated and used as input for an expert-guided classification of flood and non-flood. VH and VV-band backscatter (dB) statistics for flood and non-flood samples are presented in Figure S1. For this analysis, only two major classes, a "waterbodies" class and an "others" class, were considered. Box plots were used to show the statistical distribution of the data. A distinct separable backscatter value for water and other classes was used for image classification [44,63].

To understand the quality of the produced thematic maps, a validation process was required for the classification results [39,64]. During the flood disaster, it is challenging to conduct fieldwork for flood map validation [65]. Cloud-free Landsat-8 images (Landsat Surface Reflectance Level-2) available during the flood period (from 22 August 2017) was used for cross comparison. The Landsat-8 image acquired on 22 August 2017 was classified for flood mapping in eCognition developer using an object-based image analysis (OBIA) method called the geographic object-based image analysis (GEOBIA). The detailed methodology used to prepare the flood maps is described in [43]. Briefly, eCognition Developer software was used to divide the image into segments. The GEOBIA method

segments remote sensing imagery into meaningful image objects based on the spatial, spectral, and temporal characteristics of image pixels. During the Landsat based flood mapping, few procedures were applied in terms of selected attributes using indices such as the normalized difference water index (NDWI), normalized difference vegetation index (NDVI), a and the land and water mask (LWM) derived from spectral values of the image, together with land band information. Finally, developed rule sets exploring the image object mean value were used to generate Landsat-based flood maps. The Landsat-based flood maps are shown in Figure 4c and were used to see omission and commission errors with Sentinel-1-based flood maps. A comparison was made between Landsat and Sentinel-1-derived inundation areas. Figure 4 shows the comparison of optical data and SAR-based flood inundation maps.

In addition, 4500 reference points were collected from the Landsat-8 image of 22 August to validate the flood map of 29 August that was the closest available flood map from 22 August. The expert-guided classification scheme achieved an overall classification accuracy of 96.44%.

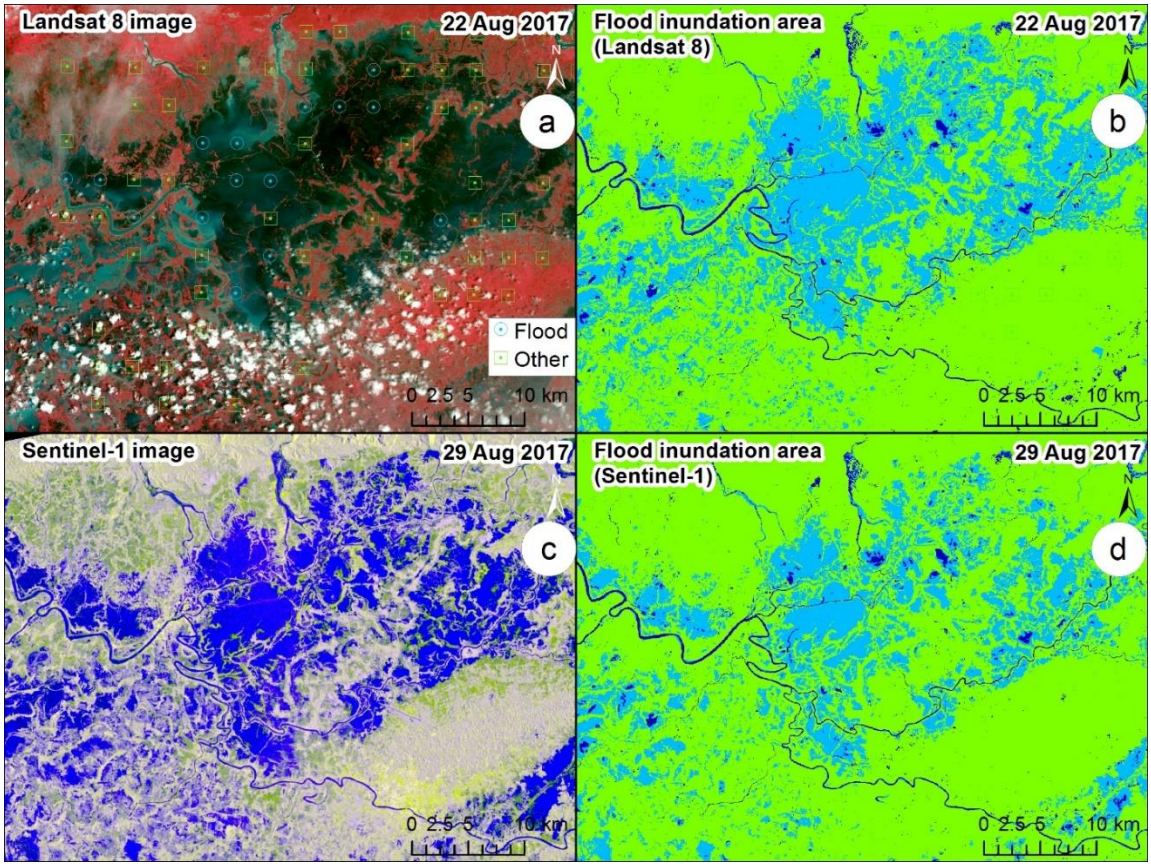

Figure 4. Comparison of optical data and synthetic aperture radar—(SAR) based flood inundation: (**a**) False color composite Landsat-8 image from 22 August 2017; (**b**) classification result based on Landsat-8 (dark blue: Perennial water; light blue: Flood inundation areas; green: Other areas); (**c**) false color composite Sentinel-1 image from 29 August 2017, showing water bodies in blue; (**d**) classification result based on Sentinel-1 data (same color assignment).

As the initially detected flood extent includes both permanent water bodies and flooded water, pre-flood water extent must be removed from the classified map of flooded area [66]. Pre-flood waterbodies classified from Landsat images acquired before 27 March 2017 was considered as perennial waterbodies because no news reports about floods were received before that date [22]. Overlaying the pre-flood waterbodies with the April, June, and August flood maps, the flood inundation area was separated from perennial water bodies. Further analysis of the derived flood information was carried

out in the ArcGIS environment to perform damage assessment as well as associated statistical analysis at a 30-m resolution (flood area estimation, affected area estimation).

As part of the flood damage assessment, pre-flood land cover maps for the year 2017 were prepared in GEE using Landsat images acquired between January and April of that year. For land cover mapping, optical satellite images were used, e.g., Landsat are most common, and data were freely accessible and are often used to explore unique spectral characteristics of different land cover using image indices. The Google Earth Engine environment is a powerful computational fast analysis processing platform that can handle huge volumes of remote sensing imagery [67,68]. GEE provides online access to archived pre-processed Landsat imagery [69]. In the GEE, a sequence of processing steps was followed (Figure 2) for image analysis and land use/land cover mapping. All the 2017 pre-flood Landsat data for the entirety of Bangladesh were processed to derive the pre-flood water extent (https://code.earthengine.google.com/). First, as part of the atmospheric image correction, a cloud-free Landsat-8 image composites were prepared using partially cloudy images available for the period of January and April 2017. Using the derived cloud free image composites, the normalized difference vegetation index (NDVI), normalized difference water index (NDWI), normalized difference moisture index (NDMI), bare soil index (BSI), normalized pigment chlorophyll ratio index (NPCRI), and land and water mask (LWM) index were created and used for land cover mapping.

A supervised classification scheme was used to generate 2017 land cover maps from the set of Landsat-8-based index layers. To facilitate the 2017 land cover classification, training data were acquired using Google Earth High-resolution images as a basis. A total of 5484 training sets were collected for areas under tree coverage (Madhupur forest, hill forest, and mangrove forest, as well as rural settlement and homestead orchard), 8 were acquired for grassland, 346 for the barren area, 1039 for cropland, 3142 for waterbodies, and 86 for built-up areas. All the land cover legends were developed based on the land cover classification system (LCCS), which was developed by FAO to provide a consistent framework for the classification and mapping of land cover [70,71]. All training data were imported into the Google Earth Engine environment in the form of a fusion table. Finally, a classification and regression tree (CART) land cover classifier was applied using the imported training sets and the Landsat-related raster layers. The CART is a decision tree (DT) based machine-learning method for constructing prediction models from a set of training data using the concept of information entropy that shows the strongly improved performance of classification [72,73]. In addition to the Landsat bands "B1", "B2", "B3", "B4", "B5", "B6", "B7", "B8", and "B9", the indices "NDVI", "NDWI", "NDMI", "BSI", "NPCRI", "LWM", and the SRTM DEM were also used in the classification. As with any digitally classified land cover product, there can be reasons for misclassification related to the environmental conditions at the time of image acquisition (clouds, fog, etc.), variations in local forest types or limitations in computational algorithms. Finally, the derived land cover maps were validated using another set of samples collected from field data and independent training data from high-resolution images of Google Earth. Publicly open earth observation data and online map tools like Google Map, Google Earth, Collect Earth Online and OpenStreetMap allow the accuracy assessment of a national level land cover based on very high-resolution satellite images [38,39,74–76]. The accuracy of the 2017 Landsat-derived land cover map was assessed using (10 km × 10 km) 1400 reference points from Google Earth and 65 points from the ground. These were compared with the land cover map to calculate the error matrix, and an overall accuracy of 87.51% was found.

3. Results

Developed national level pre and post-flood inundation maps for the entire country, during March, April, June, and August 2017, based on the Sentinel-1 images, are presented in Figure 5. The results show the presence of perennial waterbodies in March 2017 covering an area of 5.03% in Bangladesh. In April 2017, a total flood-inundated area was 2.01%, with most inundation was occurring in cropland (1.51%), followed by rural settlement and homestead orchard areas (0.21%), and other areas (0.29%).

Similarly, more areas were inundated during the catastrophic June and August 2017 months, with inundation covering 4.53% and 7.01%, respectively.

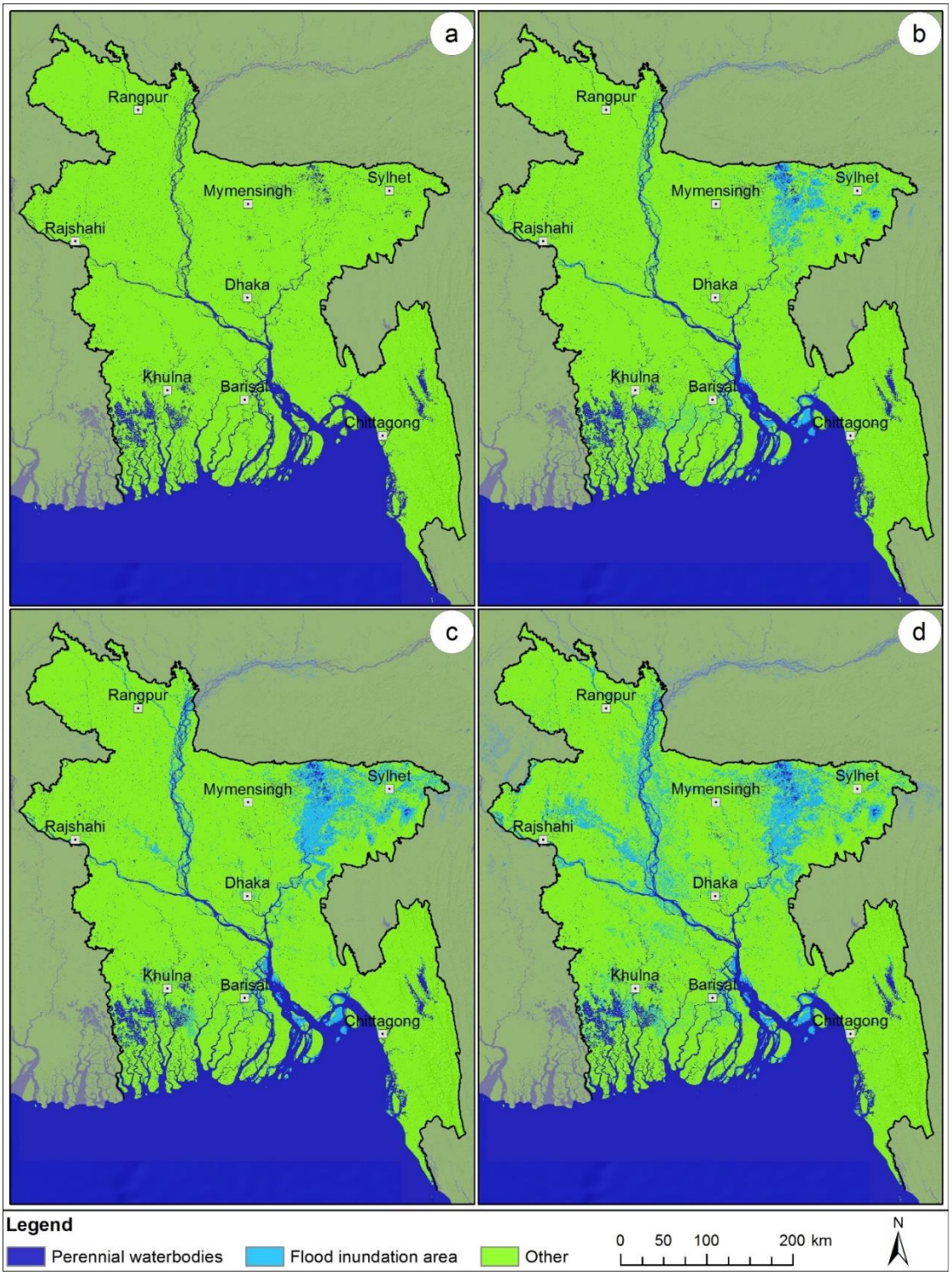

Figure 5. Comprehensive flood inundation map of Bangladesh for the months of (**a**) March, (**b**) April, (**c**) June, and (**d**) August 2017.

The 2017 flood of Bangladesh caused significant inundation of cropland, rural settlement, and homestead orchard, and other land use areas. Considering all crop-related land use and land cover

types (Figure 6), the percentage of inundated cropland was found to be 1.51%, 3.46%, and 5.30% in April, June, and August respectively. Significant inundation also occurred to residential property, public infrastructure, and fish farming ponds. A total of 0.21% of the rural settlement and homestead orchard areas were inundated in April, increasing to 0.47% in June, and 0.65% in August (Figure 7).

The time series flood data in Figure 8 shows that for the April to August 2017 time frame, some of the areas experienced continuous inundation, while some areas were progressively inundated, and some recovered from the flood waters as time progressed. Within the April and June 2017 time frame, an inundated area of 257,729 ha was common for both months, while 410,853 ha were newly flooded, and 38,776 ha recovered from the flood inundation. From June to August 2017, 532,173 ha were common for both months, while 502,927 ha were newly inundated, and 136,406 ha recovered from the floods (Figure 8).

Figure 6. 2017 land cover map of Bangladesh developed using Landsat 8 and Google Earth Engine cloud computing.

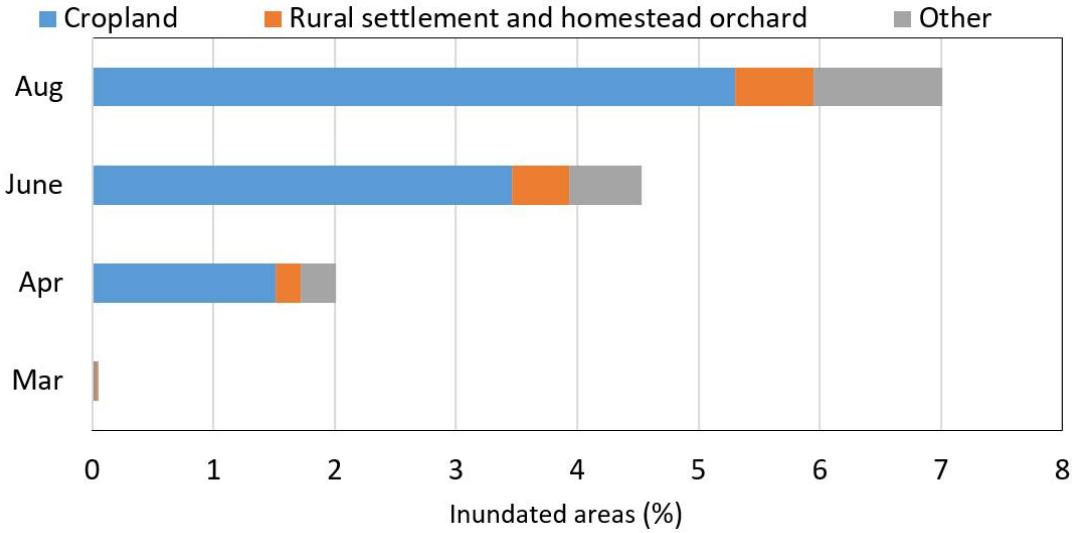

Figure 7. Flood affected major land cover categories. Flood extent was derived from Sentinel-1 SAR data while land cover classes were extracted from cloud-free Landsat-8 imagery.

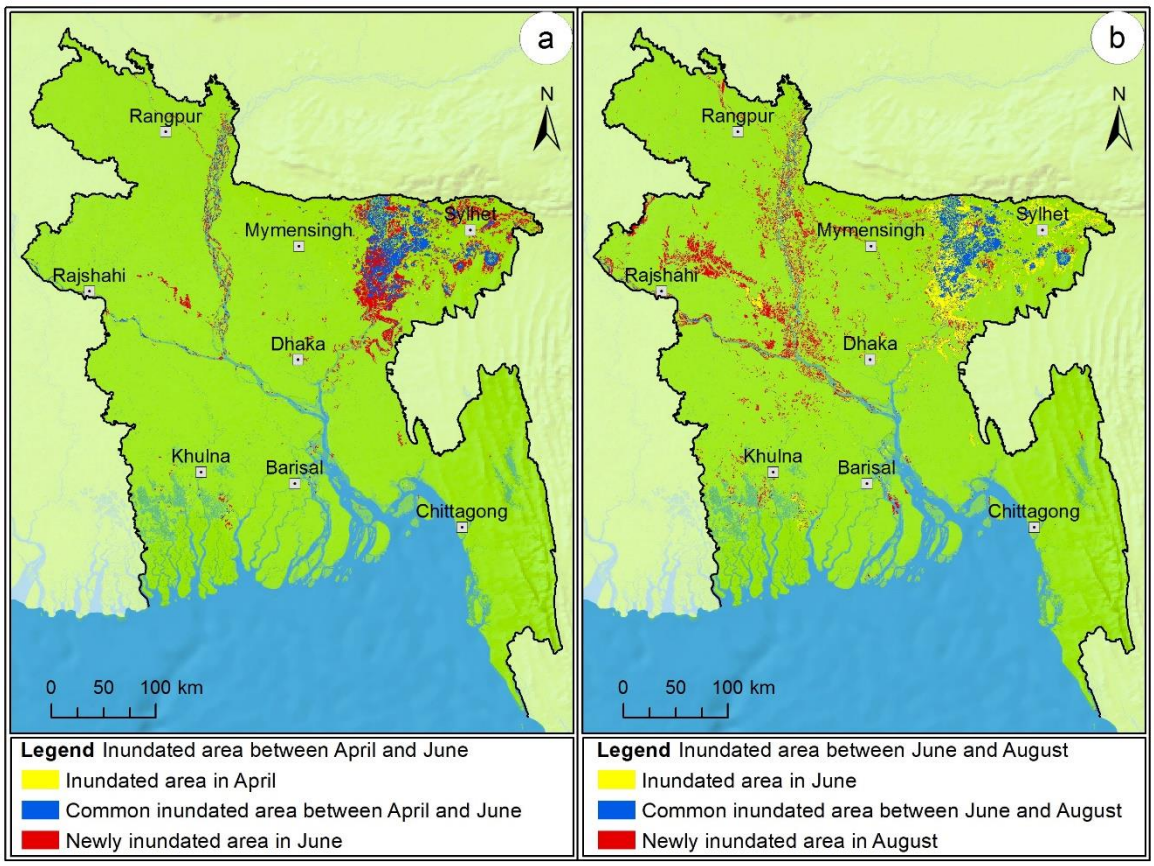

Figure 8. Flood recession and rise areas of Bangladesh between (**a**) April and June, (**b**) June and August.

A land cover map for the same year was also derived from Landsat-8 data for potential flood damage assessment. The derived map was produced from a cloud-free Landsat-8 composite between 1 January and 1 April 2017 and is shown in Figure 6. The map consists of nine classes, namely, tree cover (Madhupur forest, hill forest, and mangrove forest, as well as rural settlement and homestead orchard), grassland, cropland, barren area, built-up area, and waterbodies.

Through the possibility of an automatic SAR-based processing chain, flood inundation mapping based on Sentinel-1 images have the potential to rapidly provide flood information for flood management. During flood mapping, a significant difference in backscatter values for waterbodies and non-water areas enables a separation between inundated areas and other land areas. Derived optimal backscatter ranges for flood inundated areas in Sentinel-1 images shows a clear distinction from other classes, as presented in Figure S1. The backscatter response in VH polarizations for inundated areas were between −24.25 dB and −17.4 dB for this area of interest. In VV polarizations, water bodies showed a range between −22.4 dB and −12.9 dB. The backscatter response in VH polarizations for non-water areas was determined between −16 dB and −9.6 dB, and in VV polarizations it ranged between −10.8 dB and −1 dB. Identified optimal ranges of backscatter values can be applied for the automation of flood mapping using Sentinel-1 images to produce flood inundation maps for areas of similar topography.

For an accuracy assessment, the Sentinel-1 classification result for 29 August 2017, was evaluated with the waterbodies map derived from Landsat-8 (22 August 2017) using 4500 reference points collected from the Landsat-8 classification map. The overall accuracy of the 2017 August flood inundation map was found to be 96.44%, with a kappa value of 0.81, standard error kappa of 0.02, and a 95% confidence interval between 0.770 to 0.850 (Table 1). The evaluation of the flood map from SAR data compared to the optical image-based inundation map (Table S4) shows that for a particular cloud free window, the Landsat- (22 August 2017) based map produced an inundated area of 70% while the SAR-based map showed 59% of the areas inundated. Within the 70% Landsat-based inundated maps, a 53% inundated area was common, 17% of the area was an omission, and 6% of the area differed from the Sentinel-1-based study. A visual comparison of the Landsat-based (22 August 2017) and Sentinel-1-based (29 August 2017) flood extent is also shown in Figure 4.

Table 1. Error matrix for the land cover map of 2017.

Class Name	Flood	Other	Total	Accuracy
Flood	1335	123	1458	91.56
Other	37	3005	3042	98.78
Total	1372	3128	4500	n.a.
Producer's accuracy (%)	97.30	96.07	n.a.	n.a.

The accuracy of the 2017 Landsat-derived land cover map was found to be 87.51%, with a kappa value of 0.81, a standard error kappa of 0.02, a 95% confidence interval between 0.770 and 0.850, and a 0.906 maximum possible unweighted kappa, given the observed marginal frequencies (Table 2).

Table 2. Error matrix for the land cover map of 2017.

Land Cover	Hill Forest	Madhupur Forest	Mangrove Forest	Rural Settlement and Homestead Orchard	Grassland	Cropland	Barren Area	Built-Up Area	Waterbodies	Total	Users Accuracy (%)
Hill forest	155	1		1		8			1	166	93.37
Madhupur forest		7		1		1				9	77.78
Mangrove forest			43	1						44	97.73
Rural settlement and homestead orchard	1	1	1	214		60			2	279	76.70
Grassland			1		3		1		1	6	50.00
Cropland				59	1	722	3		12	797	90.59
Barren area						1	19	1	1	22	86.36
Built-up area				3		2		6		11	54.55
Waterbodies						18			113	131	86.26
Total	156	9	45	279	4	812	23	7	130	1465	n.a.
Producer's accuracy (%)	99.36	77.78	95.56	76.70	75.00	88.92	82.61	85.71	86.92	n.a.	n.a.

4. Discussion

It is well known that Bangladesh has a long history of natural disasters. Between 1980 and 2008, it experienced 219 natural disasters that caused over USD $16 billion in total damage [77]. Due to the flat topography and climatic features, more than 80% of the population is potentially exposed to floods. Following the devastating disaster issues, Bangladesh has made significant efforts to reduce its disaster vulnerability primarily through post-disaster management. The Government of Bangladesh (GOB) recently constructed a good number of flood shelters, built flood protection embankments, sluice gates and regulators on different rivers, and have been dredging the drainage channels and canals [78]. Compared to previous efforts, Bangladesh is now much safer from disasters due to these post-disaster actions. Another survey of published literature concluded that considerably less research has been conducted for operational flood mapping using earth observation data for emergency response. Space based earth observation (EO) data can be used to deliver information on the extent of hazards during response operations so as to mitigate damage [79].

In the past, vital research was conducted for the 1988 flood mapping to support relief operations [7]. After that, few flood mapping studies have been conducted by academic researchers related to flood issues in Bangladesh without focusing on emergency response [6,14,21,33,35,48]. Relatively, cloud-free satellite images showed that during the last three weeks of September, areas of inundation were 31% to 42% of Bangladesh. The actual flooded area was more from satellite image estimates which differed from officially reported areas [80]. Although real-time flood monitoring plays a vital role in relief operations [81,82], flood maps also play an important role in decision-making, planning, and implementing flood management options [83]. Most of the studies have published their flood mapping results ten years after a flood event [32]. Sometimes the flood duration is quite long, although many researchers have mapped flooding areas for a single month. Furthermore, no dissemination systems were implemented to support sharing the inundated area maps during the crisis or after publishing the research article [84]. A number of monitoring systems have the potential for flood management in Bangladesh, however limited access to discharge data from the upstream, and lack of timely acquisition of geospatial data has an impact on the operational suitability of these systems. In many cases, model-based inundation mapping does not provide good results on plain land area [18]. Cloudy weather also prevents optical systems to provide coherent image coverage to use for flood inundation mapping. Due to the high level of cloud contamination during the monsoon time, cloud-free Landsat images identification was difficult for flood mapping [85]. For Bangladesh, one of the best opportunities for operational flood mapping comes from Sentinel-1 imaging as it is publically available [63]. In Bangladesh, the agriculture sector is greatly impacted by floods, despite conventional flood management systems paying very limited attention to this sector [63].

Under the circumstances that Bangladesh is under, the present study provides rapid flood inundation maps for March, April, June, and August 2017 using publicly available Sentinel-1 data using a replicable methodology. The derived flood maps provide spatial and temporal dynamics of the flooding area across the county. The utilization of the GEE for image processing facility in this study helped to promptly develop an operational land cover map for damage assessment. The advanced image processing tools of GEE enables the generation of accurate land coverage for large areas without downloading bulk data and prolonged desktop processing [86]. The method can be used for monitoring land cover regularly as the analysis can easily be re-run while new Landsat data is injected in GEE. The derived maps provide crucial information for local disaster management agencies, which helps to prioritize relief and rescue operations. At the same time, automatically generated land cover maps derived from pre-flood Landsat-8 data support the assessment of economic loss and help in the prioritization of financial compensation due to crop damage. The use of SAR images provides significant advantages, as their cloud-free and all-weather capabilities enable the production of regularly sampled flood extent information in a near real-time delivery manner [7,87]. Before the launch of Sentinel-1B, the revisit time of Sentinel-1A was 12 days, which was challenging for a rapid disaster response. After the launch of Sentinel-1B and the completion of the two satellite

Sentinel-1 constellation, revisit times improved to six days over the area of interest. In the future, a constellation of three Sentinel satellites would be much more useful for responding to flooding events in near real-time. As part of this study, the team provided georeferenced GIS layers in addition to jpg-formatted maps to encourage the broad use of data and to ensure that the data are fully compliant with the GIS environments used by the response agencies [88].

For this study, the use of Sentinel-1 dual-polarization radar images showed a high potential for flood mapping due to their free-of-charge nature. Adopting the image pre-processing techniques and knowledge-based classification methods used in this study helped in developing scene-specific standards and knowledge and achieved better classification accuracy on flood maps [89,90]. For this exercise, the developed flood mapping system was run on a desktop-type computer. Hence, the availability of sufficient computing hardware and internet bandwidth were the main limitations discovered in this study. For future implementations, we will consider the utilization of cloud computing resources, such as those offered by the Google Earth Engine, the ESA Thematic Exploitation Platforms, or Amazon Web Services-based environments offered by NASA's Alaska Satellite Facility (ASF) DAAC with all Sentinel images. At the same time, utilizing recently released public-domain Landsat-8 datasets via the Google Earth Engine or similar platforms may enable the establishment of a framework for rapid land cover monitoring on a national level [40].

The present study produced a flood inundation map with optimum accuracy for the entirety of Bangladesh. However, there were some uncertainties of flood maps due to the floating vegetated areas [91]. On the Sentinel-1 images, sometimes cultivated land for rice plantation was appeared as inundated areas. To overcome those uncertainties, local knowledge is crucial. Alternatively, unmanned aerial vehicles (UAVs) are emerging tools for the monitoring of real time floods in disaster management [92]. Due to flight endurance and payload capacity, UAVs would not be functional if large areas were inundated [69]. In general, SNAP tools take a longer time for preprocessing Sentinel-1 images. There is also a lag time between the image availability in ESA Sentinel hub and in GEE. If lag time is reduced in the future, the method could be implemented in GEE environment for a more rapid production of flood extent.

Bangladesh is a flood-prone country and thus under constant threat of flooding. Every year, floods destroy lives, livestock, and infrastructure, bringing an enormous financial toll. During disasters, obtaining reliable information is crucial. As part of the operational methods, flood inundation was validated using Landsat-8 images. Unfortunately, due to the dominance of cloudy conditions, no (cloud-free) Landsat images were available during the peak flood period. Apart from wall-to-wall comparisons with optical or field-based studies, a determination of the extent of flooding in Bangladesh could serve disaster management purposes such as relief operations.

5. Conclusions

Based on the results of the study, we can conclude that earth observation and geospatial technologies provide prompt information for effective decisions for comprehensive flood disaster management for Bangladesh. Due to the predominance of severe weather conditions during flooding time, freely available and regularly sampled Sentinel-1 SAR earth observation data has great potential in producing flood information with high accuracy and high spatial resolution in a six day interval. The method was based on publicly available free-of-charge data, particularly useful for less developed countries. Cloud-based computation environments, such as the GEE platform, proved to be particularly valuable for operational users in planning a flood-related emergency response and for understanding flood damage by land cover mapping. Natural flood disasters are common and cannot be stopped. However, efficient tools for flood inundation mapping and flood damage assessment can be useful for emergency response and disaster management.

Supplementary Materials: The following are available online at http://www.mdpi.com/2072-4292/11/13/1581/s1, Figure S1. Box plots of Sentinel-1 VH and VV backscatter for flood and non-flood samples, Table S1. List of Sentinel-1 images used for the flood inundation mapping, Table S2. Landsat 8 operational land imager (OLI) spectral bandwidth spatial resolution, Table S3. Land cover classification system (LCCS) along with adopted code, Table S4. Omission and commission (%) errors between Landsat (22 August 2017) and Sentinel images (29 August 2017).

Author Contributions: K.U. and M.A.M. conceptualized overall research design; K.U. performed image analysis, prepared the flood map, land cover maps, flood damage assessment, and change assessment, and drafted the first version of the manuscript; M.A.M. and F.J.M. reviewed and provided feedback; finally all the authors read, edited, critiqued the manuscript, and approved the final version.

Acknowledgments: We express our gratitude to David Molden, Director General and Eklabya Sharma, Deputy Director General of ICIMOD for the overall guidance. This study was partially supported by core funds of ICIMOD contributed by the governments of Afghanistan, Australia, Austria, Bangladesh, Bhutan, China, India, Myanmar, Nepal, Norway, Pakistan, Switzerland, and the United Kingdom. This paper has been prepared under the SERVIR-Himalaya initiative funded by the NASA and USAID. Our special gratitude goes to Birendra Bajracharya, Chief of Party, SERVIR HKH for their encouragement and very active support in bringing out this work. Finally, we would like to thank those who reviewed the articles incomprehensibly and provided valuable suggestions to improve the manuscript.

Conflicts of Interest: The views and interpretations in this publication are those of the authors. They are not necessarily attributable to ICIMOD and do not imply the expression of any opinion by ICIMOD concerning the legal status of any country, territory, city, or area of its authority, or concerning the delimitation of its frontiers or boundaries, or the endorsement of any product.

References

1. Ozaki, M. *Disaster Risk Financing in Bangladesh*; ADB South Asia Working Paper Series No. 46; Asian Development Bank: Metro Manila, Philippines, 2016.
2. Chowdhury, R.B.; Moore, G.A. Floating agriculture: a potential cleaner production technique for climate change adaptation and sustainable community development in Bangladesh. *J. Clean. Prod.* **2017**, *150*, 371–389. [CrossRef]
3. Dasgupta, S.; Huq, M.; Khan, Z.H.; Sohel Masud, M.; Ahmed, M.M.Z.; Mukherjee, N.; Pandey, K. Climate proofing infrastructure in Bangladesh: The incremental cost of limiting future flood damage. *J. Environ. Dev.* **2011**, *20*, 167–190. [CrossRef]
4. Biswas, A.K. Management of Ganges-Brahmaputra-Meghna System: Way Forward. In *Management of Transboundary Rivers and Lakes*; Varis, O., Biswas, A.K., Tortajada, C., Eds.; Springer: Berlin/Heidelberg, Germany, 2008; pp. 143–164. [CrossRef]
5. Ahmad, Q.; Ahmed, A.U. Regional cooperation in flood management in the Ganges-Brahmaputra-Meghna region: Bangladesh perspective. In *Flood Problem and Management in South Asia*; Springer: Berlin/Heidelberg, Germany, 2003; pp. 181–198.
6. Banerjee, L. Effects of flood on agricultural productivity in Bangladesh. *Oxf. Dev. Stud.* **2010**, *38*, 339–356. [CrossRef]
7. Rasid, H.; Pramanik, M. Areal extent of the 1988 flood in Bangladesh: How much did the satellite imagery show? *Nat. Hazards* **1993**, *8*, 189–200. [CrossRef]
8. Mirza, M.M.Q. Climate change, flooding in South Asia and implications. *Reg. Environ. Chang.* **2011**, *11*, 95–107. [CrossRef]
9. Bangladesh Bureau of Statistics. *Banglaxesh Disaster Related Statistics 2015*; BBS: Dhaka, Bangladesh, 2016.
10. Mirza, M.M.Q. Global warming and changes in the probability of occurrence of floods in Bangladesh and implications. *Glob. Environ. Chang.* **2002**, *12*, 127–138. [CrossRef]
11. Kundzewicz, Z.W.; Kanae, S.; Seneviratne, S.I.; Handmer, J.; Nicholls, N.; Peduzzi, P.; Mechler, R.; Bouwer, L.M.; Arnell, N.; Mach, K.; et al. Flood risk and climate change: global and regional perspectives. *Hydrol. Sci. J.* **2014**, *59*, 1–28. [CrossRef]
12. Dash, J.; Paul, R. *Worst Monsoon Floods in Years Kill More Than 1200 across South Asia*; Reuters: London, UK, 2017.
13. Lin, L.; Di, L.; Tang, J.; Yu, E.; Zhang, C.; Rahman, M.; Shrestha, R.; Kang, L. Improvement and Validation of NASA/MODIS NRT Global Flood Mapping. *Remote Sens.* **2019**, *11*, 205. [CrossRef]

14. Chowdhury, E.H.; Hassan, Q.K. Use of remote sensing data in comprehending an extremely unusual flooding event over southwest Bangladesh. *Nat. Hazards* **2017**, *88*, 1805–1823. [CrossRef]
15. Amarnath, G.; Rajah, A. An evaluation of flood inundation mapping from MODIS and ALOS satellites for Pakistan. *Geomat. Nat. Hazards Risk* **2016**, *7*, 1526–1537. [CrossRef]
16. Shen, X.; Wang, D.; Mao, K.; Anagnostou, E.; Hong, Y. Inundation Extent Mapping by Synthetic Aperture Radar: A Review. *Remote Sens.* **2019**, *11*, 879. [CrossRef]
17. Bates, P.D. Remote sensing and flood inundation modelling. *Hydrol. Process.* **2004**, *18*, 2593–2597. [CrossRef]
18. Jung, Y.; Kim, D.; Kim, D.; Kim, M.; Lee, S. Simplified flood inundation mapping based on flood elevation-discharge rating curves using satellite images in gauged watersheds. *Water* **2014**, *6*, 1280–1299. [CrossRef]
19. Rahman, M.S.; Di, L. The state of the art of spaceborne remote sensing in flood management. *Nat. Hazards* **2017**, *85*, 1223–1248. [CrossRef]
20. Chowdhury, M.R. Consensus seasonal Flood Forecasts and Warning Response System (FFWRS): An alternate for nonstructural flood management in Bangladesh. *Environ. Manag.* **2005**, *35*, 716–725. [CrossRef] [PubMed]
21. Islam, A.S.; Bala, S.K.; Haque, M. Flood inundation map of Bangladesh using MODIS time-series images. *J. Flood Risk Manag.* **2010**, *3*, 210–222. [CrossRef]
22. Ahmed, M.R.; Rahaman, K.R.; Kok, A.; Hassan, Q.K. Remote Sensing-Based Quantification of the Impact of Flash Flooding on the Rice Production: A Case Study over Northeastern Bangladesh. *Sensors* **2017**, *17*, 2347. [CrossRef]
23. Rahman, M.S.; Di, L.; Shrestha, R.; Eugene, G.Y.; Lin, L.; Zhang, C.; Hu, L.; Tang, J.; Yang, Z. Agriculture flood mapping with Soil Moisture Active Passive (SMAP) data: A case of 2016 Louisiana flood. In Proceedings of the 2017 6th International Conference on Agro-Geoinformatics, Fairfax, VA, USA, 7–10 August 2017; pp. 1–6.
24. Joyce, K.E.; Belliss, S.E.; Samsonov, S.V.; McNeill, S.J.; Glassey, P.J. A review of the status of satellite remote sensing and image processing techniques for mapping natural hazards and disasters. *Prog. Phys. Geogr.* **2009**, *33*, 183–207. [CrossRef]
25. Nandi, I.; Srivastava, P.K.; Shah, K. Floodplain Mapping through Support Vector Machine and Optical/Infrared Images from Landsat 8 OLI/TIRS Sensors: Case Study from Varanasi. *Water Resour. Manag.* **2017**, *31*, 1157–1171. [CrossRef]
26. Doody, T.; Overton, I.; Pollock, D. Floodplain inundation mapping. In *Ecological Outcomes of Flow Regimes in the Murray–Darling Basin*; Report Prepared for the National Water Commission by CSIRO Water for a Healthy Country Flagship; Overton, I., Colloff, M.J., Doody, T.M., Henderson, B., Cuddy, S.M., Eds.; CSIRO: Canberra, Australia, 2009; pp. 289–308.
27. Wilson, A.M.; Jetz, W. Remotely sensed high-resolution global cloud dynamics for predicting ecosystem and biodiversity distributions. *PLoS Biol.* **2016**, *14*, e1002415. [CrossRef]
28. Greifeneder, F.; Wagner, W.; Sabel, D.; Naeimi, V. Suitability of SAR imagery for automatic flood mapping in the Lower Mekong Basin. *Int. J. Remote Sens.* **2014**, *35*, 2857–2874. [CrossRef]
29. Ajmar, A.; Boccardo, P.; Broglia, M.; Kucera, J.; Giulio-Tonolo, F.; Wania, A. Response to Flood Events: The Role of Satellite-Based Emergency Mapping and the Experience of the Copernicus Emergency Management Service. *Flood Damage Surv. Assess. New Insights Res. Pract.* **2017**, *228*, 213–228.
30. Ohki, M.; Watanabe, M.; Natsuaki, R.; Motohka, T.; Nagai, H.; Tadono, T.; Suzuki, S.; Ishii, K.; Itoh, T.; Yamanokuchi, T. Flood Area Detection Using ALOS-2 PALSAR-2 Data for the 2015Heavy Rainfall Disaster in the Kanto and Tohoku Area, Japan. *J. Remote Sens. Soc. Jpn.* **2016**, *36*, 348–359.
31. Voormansik, K.; Praks, J.; Antropov, O.; Jagomagi, J.; Zalite, K. Flood mapping with TerraSAR-X in forested regions in Estonia. *IEEE J. Sel. Top. Appl. Earth Obs. Remote Sens.* **2014**, *7*, 562–577. [CrossRef]
32. Hoque, R.; Nakayama, D.; Matsuyama, H.; Matsumoto, J. Flood monitoring, mapping and assessing capabilities using RADARSAT remote sensing, GIS and ground data for Bangladesh. *Nat. Hazards* **2011**, *57*, 525–548. [CrossRef]
33. Werle, D.; Martin, T.C.; Hasan, K. Flood and Coastal Zone Monitoring in Bangladesh with Radarsat ScanSAR: Technical Experience and Institutional Challenges. *Johns Hopkins APL Tech. Dig.* **2000**, *21*, 148–154.
34. Dewan, A.M.; Islam, M.M.; Kumamoto, T.; Nishigaki, M. Evaluating flood hazard for land-use planning in Greater Dhaka of Bangladesh using remote sensing and GIS techniques. *Water Resour. Manag.* **2007**, *21*, 1601–1612. [CrossRef]

35. Roy, S.K.; Sarker, S.C. Integration of Remote Sensing Data and GIS Tools for Accurate Mapping of Flooded Area of Kurigram, Bangladesh. *J. Geogr. Inf. Syst.* **2016**, *8*, 184. [CrossRef]
36. Uddin, K.; Guring, D.R. Land cover change in Bangladesh: A knowledge based classification approach. In Proceedings of the 10th International Symposium on Hill Mountain Remote Sensing Cartography, Kathmandu, Nepal, 8–11 September 2008.
37. Gilani, H.; Shrestha, H.L.; Murthy, M.; Phuntso, P.; Pradhan, S.; Bajracharya, B.; Shrestha, B. Decadal land cover change dynamics in Bhutan. *J. Environ. Manag.* **2015**, *148*, 91–100. [CrossRef]
38. Uddin, K.; Abdul Matin, M.; Maharjan, S. Assessment of Land Cover Change and Its Impact on Changes in Soil Erosion Risk in Nepal. *Sustainability* **2018**, *10*, 4715. [CrossRef]
39. Uddin, K.; Shrestha, H.L.; Murthy, M.; Bajracharya, B.; Shrestha, B.; Gilani, H.; Pradhan, S.; Dangol, B. Development of 2010 national land cover database for the Nepal. *J. Environ. Manag.* **2015**, *148*, 82–90. [CrossRef] [PubMed]
40. Huang, H.; Chen, Y.; Clinton, N.; Wang, J.; Wang, X.; Liu, C.; Gong, P.; Yang, J.; Bai, Y.; Zheng, Y. Mapping major land cover dynamics in Beijing using all Landsat images in Google Earth Engine. *Remote Sens. Environ.* **2017**, *202*, 166–176. [CrossRef]
41. Xiong, J.; Thenkabail, P.; Tilton, J.; Gumma, M.; Teluguntla, P.; Oliphant, A.; Congalton, R.; Yadav, K.; Gorelick, N. Nominal 30-m cropland extent map of continental Africa by integrating pixel-based and object-based algorithms using Sentinel-2 and Landsat-8 data on Google Earth Engine. *Remote Sens.* **2017**, *9*, 1065. [CrossRef]
42. Hansen, M.C.; Potapov, P.V.; Moore, R.; Hancher, M.; Turubanova, S.; Tyukavina, A.; Thau, D.; Stehman, S.; Goetz, S.; Loveland, T.R. High-resolution global maps of 21st-century forest cover change. *Science* **2013**, *342*, 850–853. [CrossRef] [PubMed]
43. Uddin, K.; Gurung, D.R.; Giriraj, A.; Shrestha, B. Application of Remote Sensing and GIS for Flood Hazard Management: A Case Study from Sindh Province, Pakistan. *Am. J. Geogr. Inf. Syst.* **2013**, *2*, 1–5.
44. Manjusree, P.; Kumar, L.P.; Bhatt, C.M.; Rao, G.S.; Bhanumurthy, V. Optimization of threshold ranges for rapid flood inundation mapping by evaluating backscatter profiles of high incidence angle SAR images. *Int. J. Disaster Risk Sci.* **2012**, *3*, 113–122. [CrossRef]
45. Syed, M.A.; Al Amin, M. Geospatial modeling for investigating spatial pattern and change trend of temperature and rainfall. *Climate* **2016**, *4*, 21. [CrossRef]
46. WorldAtlas. 10 Largest Rice Producing Countries. Available online: https://www.worldatlas.com/articles/the-countries-producing-the-most-rice-in-the-world.html (accessed on 25 June 2018).
47. Temps, C. Rainfall/Precipitation in Dhaka, Bangladesh. Available online: https://en.climate-data.org/asia/bangladesh/dhaka-division/dhaka-1062098/ (accessed on 17 June 2018).
48. Paul, B.K.; Rasid, H. Flood damage to rice crop in Bangladesh. *Geogr. Rev.* **1993**, *83*, 150–159. [CrossRef]
49. NASA. NASA Shuttle Radar Topography Mission Global 1 Arc Second. Available online: https://cgiarcsi.community/data/srtm-90m-digital-elevation-database-v4-1/ (accessed on 17 June 2018).
50. Haklay, M.; Weber, P. Openstreetmap: User-generated street maps. *IEEE Pervasive Comput.* **2008**, *7*, 12–18. [CrossRef]
51. Global Administrative Areas. GADM Database of Global Administrative Areas, Version 2.0. Available online: http://www.gadm.org (accessed on 25 June 2018).
52. Small, D. Flattening gamma: Radiometric terrain correction for SAR imagery. *IEEE Trans. Geosci. Remote Sens.* **2011**, *49*, 3081–3093. [CrossRef]
53. Ajadi, O.A.; Meyer, F.J.; Webley, P.W. Change detection in synthetic aperture radar images using a multiscale-driven approach. *Remote Sens.* **2016**, *8*, 482. [CrossRef]
54. Janssen, L.L.; Middelkoop, H. Knowledge-based crop classification of a Landsat Thematic Mapper image. *Int. J. Remote Sens.* **1992**, *13*, 2827–2837. [CrossRef]
55. Mwaniki, M.W.; Matthias, M.S.; Schellmann, G. Application of remote sensing technologies to map the structural geology of central Region of Kenya. *IEEE J. Sel. Top. Appl. Earth Obs. Remote Sens.* **2015**, *8*, 1855–1867. [CrossRef]
56. Gan, G.; Ma, C.; Wu, J. *Data Clustering: Theory, Algorithms, and Applications*; Society for Industrial and Applied Mathematics: Ontario, Canada, 2007; Volume 20.
57. Ghosh, A.; Mishra, N.S.; Ghosh, S. Fuzzy clustering algorithms for unsupervised change detection in remote sensing images. *Inf. Sci.* **2011**, *181*, 699–715. [CrossRef]

58. Mather, P.; Tso, B. *Classification Methods for Remotely Sensed Data*; CRC Press: Boca Raton, FL, USA, 2016.
59. Mohamed, I.N.; Verstraeten, G. Analyzing dune dynamics at the dune-field scale based on multi-temporal analysis of Landsat-TM images. *Remote Sens. Environ.* **2012**, *119*, 105–117. [CrossRef]
60. Komac, M. A landslide susceptibility model using the analytical hierarchy process method and multivariate statistics in perialpine Slovenia. *Geomorphology* **2006**, *74*, 17–28. [CrossRef]
61. Mahi, H.; Farhi, N.; Labed, K. Unsupervised classification of satellite images using K-Harmonic Means Algorithm and Cluster Validity Index. *EARSeL eProc.* **2016**, *15*, 10.
62. Kumar, G.; Sarthi, P.P.; Ranjan, P.; Rajesh, R. Performance of k-means based Satellite Image Clustering in RGB and HSV Color Space. In Proceedings of the 2016 International Conference on Recent Trends in Information Technology (ICRTIT), Chennai, India, 8–9 April 2016; pp. 1–5.
63. Rahman, M.; Di, L.; Yu, E.; Lin, L.; Zhang, C.; Tang, J. Rapid Flood Progress Monitoring in Cropland with NASA SMAP. *Remote Sens.* **2019**, *11*, 191. [CrossRef]
64. Khatami, R.; Mountrakis, G.; Stehman, S.V. Mapping per-pixel predicted accuracy of classified remote sensing images. *Remote Sens. Environ.* **2017**, *191*, 156–167. [CrossRef]
65. Wing, O.E.; Bates, P.D.; Sampson, C.C.; Smith, A.M.; Johnson, K.A.; Erickson, T.A. Validation of a 30 m resolution flood hazard model of the conterminous United States. *Water Resour. Res.* **2017**, *53*, 7968–7986. [CrossRef]
66. Jain, S.K.; Saraf, A.K.; Goswami, A.; Ahmad, T. Flood inundation mapping using NOAA AVHRR data. *Water Resour. Manag.* **2006**, *20*, 949–959. [CrossRef]
67. Firpi, O.A.A. Satellite Data for All? Review of Google Earth Engine for Archaeological Remote Sensing. *Internet Archaeol.* **2016**. [CrossRef]
68. Shelestov, A.; Lavreniuk, M.; Kussul, N.; Novikov, A.; Skakun, S. Exploring Google Earth Engine Platform for Big Data Processing: Classification of Multi-Temporal Satellite Imagery for Crop Mapping. *Front. Earth Sci.* **2017**, *5*, 17. [CrossRef]
69. Mesas-Carrascosa, F.-J.; Torres-Sánchez, J.; Clavero-Rumbao, I.; García-Ferrer, A.; Peña, J.-M.; Borra-Serrano, I.; López-Granados, F. Assessing optimal flight parameters for generating accurate multispectral orthomosaicks by UAV to support site-specific crop management. *Remote Sens.* **2015**, *7*, 12793–12814. [CrossRef]
70. Bajracharya, B.; Uddin, K.; Chettri, N.; Shrestha, B.; Siddiqui, S.A. Understanding Land Cover Change Using a Harmonized Classification System in the Himalaya. *Mt. Res. Dev.* **2010**, *30*, 143–156. [CrossRef]
71. Gregorio, A.D. *Land Cover Classification System Classification Concepts and User Manual Software Version (2)*; Food and Agriculture Organization of the United Nations: Rome, Italy, 2005.
72. Loh, W.Y. Classification and regression trees. *Wiley Interdiscip. Rev. Data Min. Knowl. Discov.* **2011**, *1*, 14–23. [CrossRef]
73. Goldblatt, R.; You, W.; Hanson, G.; Khandelwal, A.K. Detecting the boundaries of urban areas in India: A dataset for pixel-based image classification in Google Earth Engine. *Remote Sens.* **2016**, *8*, 634. [CrossRef]
74. Uddin, K.; Chaudhary, S.; Chettri, N.; Kotru, R.; Murthy, M.; Chaudhary, R.P.; Ning, W.; Shrestha, S.M.; Gautam, S.K. The changing land cover and fragmenting forest on the Roof of the World: A case study in Nepal's Kailash Sacred Landscape. *Landsc. Urban Plan.* **2015**, *141*, 1–10. [CrossRef]
75. Aguirre-Gutiérrez, J.; Seijmonsbergen, A.C.; Duivenvoorden, J.F. Optimizing land cover classification accuracy for change detection, a combined pixel-based and object-based approach in a mountainous area in Mexico. *Appl. Geogr.* **2012**, *34*, 29–37. [CrossRef]
76. Saah, D.; Johnson, G.; Ashmall, B.; Tondapu, G.; Tenneson, K.; Patterson, M.; Poortinga, A.; Markert, K.; Quyen, N.H.; San Aung, K. Collect Earth: An online tool for systematic reference data collection in land cover and use applications. *Environ. Model. Softw.* **2019**, *118*, 166–171. [CrossRef]
77. UNDP. Bangladesh: Disaster Risk Reduction as Development. Available online: https://www.undp.org/content/undp/en/home/librarypage/poverty-reduction/supporting_transformationalchange/Bangladesh-drr-casestudy-transformational-change.html (accessed on 29 June 2018).
78. Dewan, T.H. Societal impacts and vulnerability to floods in Bangladesh and Nepal. *Weather Clim. Extrem.* **2015**, *7*, 36–42. [CrossRef]
79. Zoka, M.; Psomiadis, E.; Dercas, N. The Complementary Use of Optical and SAR Data in Monitoring Flood Events and Their Effects. *Proceedings* **2018**, *2*, 644. [CrossRef]

80. Falter, D.; Schröter, K.; Dung, N.V.; Vorogushyn, S.; Kreibich, H.; Hundecha, Y.; Apel, H.; Merz, B. Spatially coherent flood risk assessment based on long-term continuous simulation with a coupled model chain. *J. Hydrol.* **2015**, *524*, 182–193. [CrossRef]
81. Borah, S.B.; Sivasankar, T.; Ramya, M.; Raju, P. Flood inundation mapping and monitoring in Kaziranga National Park, Assam using Sentinel-1 SAR data. *Environ. Monit. Assess.* **2018**, *190*, 520. [CrossRef] [PubMed]
82. Atijosan, A.; Salau, A.O.; Badru, R.A.; Alaga, T. Development of a Low Cost Community Based Real Time Flood Monitoring and Early Warning System. *Int. J. Sci. Res. Sci. Eng. Technol.* **2017**, *3*, 189–195.
83. World Meteorological Organization. *Integrated Flood Management Tools Series*; No. 20; WMO: Zurich, Switzerland, 2013; pp. 1–88.
84. Amir, M.; Khan, M.; Rasul, M.; Sharma, R.; Akram, F. Hydrologic and hydrodynamic modelling of extreme flood events to assess the impact of climate change in a large basin with limited data. *J. Flood Risk Manag.* **2018**, *11*, S147–S157. [CrossRef]
85. Klemas, V. Remote Sensing of Floods and Flood-Prone Areas: An Overview. *J. Coast. Res.* **2014**, *31*, 1005–1013. [CrossRef]
86. Zurqani, H.A.; Post, C.J.; Mikhailova, E.A.; Schlautman, M.A.; Sharp, J.L. Geospatial analysis of land use change in the Savannah River Basin using Google Earth Engine. *Int. J. Appl. Earth Obs. Geoinf.* **2018**, *69*, 175–185. [CrossRef]
87. Reiche, J.; Hamunyela, E.; Verbesselt, J.; Hoekman, D.; Herold, M. Improving near-real time deforestation monitoring in tropical dry forests by combining dense Sentinel-1 time series with Landsat and ALOS-2 PALSAR-2. *Remote Sens. Environ.* **2018**, *204*, 147–161. [CrossRef]
88. WFP. *Terai Flood 72 Hour Assessment*; Version 1; The United Nations World Food Programme, Ed.; WFP: Kathmandu, Nepal, 2017.
89. Lobry, S.; Denis, L.; Tupin, F.; Fjørtoft, R. Double MRF for water classification in SAR images by joint detection and reflectivity estimation. In Proceedings of the 2017 IEEE International Geoscience and Remote Sensing Symposium (IGARSS), Fort Worth, TX, USA, 23–28 July 2017.
90. Ban, Y.; Hu, H.; Rangel, I.M. Fusion of Quickbird MS and RADARSAT SAR data for urban land-cover mapping: Object-based and knowledge-based approach. *Int. J. Remote Sens.* **2010**, *31*, 1391–1410. [CrossRef]
91. Tsyganskaya, V.; Martinis, S.; Marzahn, P.; Ludwig, R. SAR-based detection of flooded vegetation—A review of characteristics and approaches. *Int. J. Remote Sens.* **2018**, *39*, 2255–2293. [CrossRef]
92. Casado, M.R.; Irvine, T.; Johnson, S.; Yu, D.; Butler, J. Drone watch: UAVs for flood extent mapping and damage assessment. In Proceedings of the Small Unmanned Aerial Systems for Environmental Research, Worcester, UK, 28–29 June 2018.